

Controlled magnetic properties of Ni nanoparticles embedded in polyimide films

Satoshi Tomita,^{1,*} Petra E. Jönsson,^{2,†} Kensuke Akamatsu,^{3,4} Hidemi Nawafune,³ and Hajime Takayama²

¹Graduate School of Materials Science, Nara Institute of Science and Technology, 8916-5 Takayama, Ikoma, Nara 630-0192, Japan

²Institute for Solid State Physics, University of Tokyo, 5-1-5 Kashiwa-no-ha, Kashiwa, Chiba 277-8581, Japan

³Faculty of Science and Engineering, Konan University, 8-9-1 Okamoto, Higashi-Nada, Kobe 658-8501, Japan

⁴PRESTO, Japan Science and Technology Agency, 4-1-8 Honcho, Kawaguchi, Saitama 332-0012, Japan

(Received 18 May 2007; published 20 November 2007)

We have studied the magnetic properties of Ni nanoparticles incorporated in polyimide films using dc- and ac-magnetization measurements. Transmission electron microscopy images reveal that both the mean particle diameter (d_{ave}) and the volume fraction of particles (η_{ave}) in the composite layer can be controlled independently. In a series of samples with fixed d_{ave} , the system with the lowest η_{ave} behaves magnetically as an ensemble of noninteracting superparamagnets. With increasing η_{ave} , typical signatures of the dipole-dipole interparticle interaction, such as an enhanced blocking temperature, are observed. In dense systems, with a particle concentration above the threshold for geometrical percolation, the magnetic response is ferromagnetic due to the exchange interaction between particles in direct contact.

DOI: 10.1103/PhysRevB.76.174432

PACS number(s): 75.50.Tt, 75.75.+a, 81.07.-b

I. INTRODUCTION

Ferromagnetic-metal nanoparticles are good model systems for studying how a reduction in size changes the properties of a magnetic material. It is energetically favorable for a particle smaller than a specific size to form only one magnetic domain, i.e., to become a magnetic single-domain particle.¹ Single-domain ferromagnetic-metal nanoparticles have received considerable interest due to their important technological applications mainly in high-density magnetic storage,² but also other applications based on collective magnetic behavior have been proposed.^{3,4} Moreover, an interest within basic condensed matter physics concerns magnetic dynamics and relaxation behavior of nanoparticle ensembles.^{5,6,8,7,9}

For systems of magnetically isolated nanoparticles with negligible interparticle interactions, the magnetic properties are determined by the magnetic anisotropy of each nanoparticle originating either from the magnetocrystalline anisotropy, a nonspherical particle shape, or surface effects. For any real system, dipolar interparticle interactions are inevitable and how to correctly model the magnetic relaxation of dipolar-coupled nanoparticle systems is a matter of debate.^{5-7,10} While simplified models have been proposed to understand the effects of weak to intermediate dipolar interactions, a dense nanoparticle system is, in general, a disordered system with random anisotropy and competing magnetic interaction. Such a strongly dipolar-coupled nanoparticle systems may have a rich variety of magnetic configuration with competing energy terms resulting in superspin-glass dynamics.¹¹⁻¹⁶ In order to understand the physics underlying the collective phenomena of magnetic nanoparticle systems, experiments on well characterized nanoparticle model systems, in which the interparticle interaction can be tuned precisely, are crucial.

The magnetic interparticle interaction in a ferromagnetic-metal nanoparticle system is determined by both particle diameter (d) and interparticle spacing (r). The dipolar interaction is ubiquitous, while close contacts between

nanoparticles lead to direct exchange. Electron beam lithography has been considered to be one of the best ways to fabricate magnetic microstructures with highly controlled d and r . The smallest d and r in the state-of-the-art lithographic technique are, however, limited to several tens of nanometers despite the demand for further miniaturization. Over the past few years, remarkable progress has been made in the preparation of very small structures at scales beyond the current limits of the lithographic technique by using, for example, chemical decomposition,² sputtering,^{7,17} and thermal deposition.¹⁸ Nevertheless, independent and precise tuning of d and r at the level of several nanometers still remains a challenge.

Frozen ferrofluids have often been used as model systems to study fundamental properties of magnetic-metal nanoparticles. It is, however, difficult to increase the nanoparticle volume fraction (η) uniformly and continuously; particles may form long chains or other types of aggregates. By using a sputtering technique, well characterized nanometer-sized magnetic clusters have recently been prepared.^{7,17,19} Luis *et al.*⁷ reported that sequential depositions of Al₂O₃ and Co layers bring about granular multilayers, in which the strength of interactions between the Co clusters is controlled by varying the number of layers and their separation. Such a system is ideal for studying phenomena related to two-dimensional–three-dimensional (3D) crossover. However, it is difficult to uniformly and continuously vary the particle concentration for tailoring a 3D system with any strength of the dipolar coupling from magnetically isolated to strongly interacting.

Very recently, we have embedded metallic Ni particles several nanometers in diameter in a polymer film, namely, polyimide (PI).²⁰ Structural analysis based on transmission electron microscopy (TEM) has demonstrated that d of the nanoparticles remains constant while η is increased by shrinking the PI matrix. Since $\eta \propto (d/r)^3$, this enables us to monotonically decrease r , leading to a fine tune of the interparticle interaction in the Ni nanoparticle system.²¹ It is thus possible to carry out a systematic study of the magnetic dynamics for 3D systems of single-domain Ni nanoparticles

with η varying from a few percent to above the threshold for geometrical percolation.

We will, in this paper, show that it is possible to control the magnetic properties of ferromagnetic-metal nanoparticle systems by using the Ni nanoparticles embedded in PI matrices. For this purpose, ac- and dc-magnetization measurements are carried out to probe the magnetization dynamics on well defined Ni nanoparticles characterized by TEM. We demonstrate that the magnetic properties of such Ni nanoparticle systems can be tuned from superparamagnetic to ferromagnetic by increasing the volume concentration of nanoparticles to above the percolation threshold.

II. EXPERIMENTAL DETAILS

PI films (Kapton 200-H) were first modified with aqueous potassium hydroxide (KOH) of 5 mol/dm^3 . We prepared two series of samples, one modified by KOH for 2 min (series I) and the other for 7 min (series II). The surface modified films were subsequently immersed in aqueous nickel chloride (NiCl_2) of 50 mmol/dm^3 in order to adsorb Ni^{2+} . The amount of adsorbed Ni^{2+} (N) evaluated through inductively coupled plasma atomic emission spectroscopy is $607 \times 10^{-9} \text{ mol/cm}^2$ for series I and is $1973 \times 10^{-9} \text{ mol/cm}^2$ for series II. The adsorption of Ni^{2+} was followed by thermal annealing in H_2 gas. The temperature was elevated from room temperature (RT) to $300 \text{ }^\circ\text{C}$ by $10 \text{ }^\circ\text{C/min}$ and kept for 0–130 min at $300 \text{ }^\circ\text{C}$. The Ni^{2+} were almost completely reduced to Ni atoms at $300 \text{ }^\circ\text{C}$ and Ni nanoparticles were grown,²² yielding surface nanocomposite layers consisting of Ni nanoparticles embedded in PI matrices.

The cross sections of the films were observed using TEM operated at 200 kV. Specimens for the cross-sectional TEM studies (100 nm in thickness) were prepared by the standard procedure that includes an embedding of the films in epoxy resin and a sectioning with ultramicrotome. dc- and ac-magnetization measurements at temperature ranging from 5 to 300 K were carried out using a superconducting quantum interference device magnetometer. The magnetic field was applied up to $\pm 7 \text{ T}$ in the direction parallel to the film surface. The ac magnetization was studied at frequencies ranging from 0.17 to 170 Hz.

III. RESULTS AND DISCUSSION

A. Sample characterization

Figure 1(a) shows a cross-sectional TEM image of the surface nanocomposite layer for the film in series II annealed at $300 \text{ }^\circ\text{C}$ for 30 min. We see nearly spherical Ni particles dispersed in the film. A selected-area electron diffraction pattern was assigned to fcc-Ni (not shown here). Figure 1(b) shows the size distribution of Ni particles determined from TEM pictures. The average particle diameter (d_{ave}) is 7.5 nm, and the standard deviation (σ) is 1.1 nm, indicating a narrow size distribution. Figure 1(c) shows a TEM image of a sample in series II annealed for 130 min at the same temperature. We see that the shape of the particles does not change after longer annealing. The size distribution of the nanoparticles is presented in Fig. 1(d). The d_{ave} and σ are

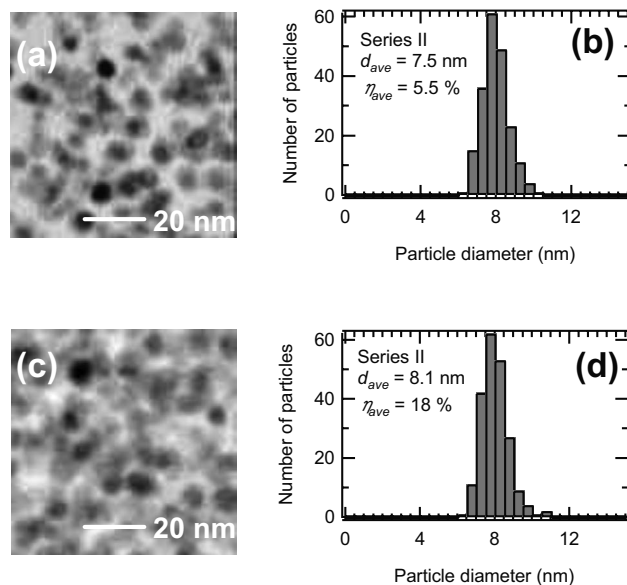


FIG. 1. Cross-sectional TEM images of the films in series II annealed at $300 \text{ }^\circ\text{C}$ for (a) 30 min with $\eta_{ave}=5.5\%$ and (c) 130 min with $\eta_{ave}=18\%$. [(b) and (d)] Size distribution of the Ni particles observed in (a) and (c), respectively.

evaluated to be 8.1 and 1.0 nm, respectively. These values are almost the same as those in Fig. 1(b).

It is worth noting here that the concentration of nanoparticles observed in Fig. 1(c) seems to be higher than that in Fig. 1(a). We have revealed that the thickness of the composite layer (t_{ave}) decreases as the annealing time increases. This is due to the volume loss of the PI matrix by the thermal decomposition.²⁰ Using t_{ave} (μm), N , the atomic weight of Ni (58.7), and the density of bulk fcc-Ni (8.91 g/cm^3), the average volume fraction η_{ave} (%) is calculated using $\eta_{ave} = (N \times 58.7 \times 100) / (t_{ave} \times 8.91 \times 10^{-4})$. Since N , the amount of adsorbed Ni^{2+} , is constant for all the films in a series of samples, a decrease in t_{ave} with increasing the annealing time brings about an increase in η_{ave} .

The estimated d_{ave} and η_{ave} for all series II samples are summarized in Table I. The η_{ave} of the nanoparticles increases from 3.2% to 18% as the annealing time increases from 0 to 130 min. The nanoparticles, however, maintain a fixed diameter d_{ave} of about 8 nm within the error of estimation. For series I samples, we obtained a similar result. The

TABLE I. Microstructures of series II samples.

Annealing time (min)	d_{ave} (nm)	η_{ave} (%)
0	7.6 ± 1.2	3.2
30	7.5 ± 1.1	5.5
60	7.5 ± 1.0	7.7
80	8.1 ± 1.0	10
120	8.4 ± 1.1	12
130	8.1 ± 1.0	18
≥ 180	Continuous Ni film	

TABLE II. Microstructures of series I samples.

Annealing time (min)	d_{ave} (nm)	η_{ave} (%)
0	4.9 ± 0.8	3.0
30	5.4 ± 1.0	5.6
60	5.6 ± 0.8	15
80	5.0 ± 0.7	23
90	5.1 ± 0.6	34
≥ 100	Continuous Ni film	

particles which maintain a diameter of 5 nm were embedded in PI with η_{ave} ranging from 3.0% to 34% as seen in Table II. These results clearly suggest that we have succeeded in controlling d_{ave} and η_{ave} independently in the Ni nanoparticle systems. We found that d_{ave} is dependent on the time of the initial KOH treatment, i.e., longer KOH treatment time brings about larger Ni nanoparticles, and on the temperature during annealing but is independent of the annealing time.²²

During annealing at 300 °C, the hydrogen-induced reduction of Ni²⁺ is accompanied by diffusion and aggregation of Ni atoms in the PI matrices to form Ni nanoparticles.²³ A smaller nanoparticle is less stable owing to a larger surface energy. Larger nanoparticles are thus grown at the expense of smaller particles within a so-called Ostwald ripening process, which includes dissolution of smaller nanoparticles and rediffusion of Ni atoms.²⁴ It is thought that when the surface energy of nanoparticles with a specific size balances the thermal energy, the nanoparticles become stable. After the formation of stable nanoparticles, they do not coalesce because the temperature is lower than the glass transition temperature of the PI matrix ($T_g=400$ °C) and the mobility of the particles is quite low in the rigid PI matrix. This explains why d_{ave} is independent of the annealing time.

For annealing times ≥ 100 min for series I and ≥ 180 min for series II, we see a continuous Ni film in TEM images, indicating that geometrical percolation is reached. The percolation threshold, at which a continuous path exists from one end of the sample to the other, is theoretically 31% for site percolation on a simple cubic lattice.²⁵

B. Magnetic properties

Figure 2(a) shows the temperature dependence of the in- and out-of-phase components of the ac susceptibility (χ' and χ'') of the film with $\eta_{ave}=5.5\%$ in series II. The measurements were carried out with a probing field of 4 Oe in the frequency range between 0.17 and 170 Hz after cooling in zero field from RT. We see that the peaks in both χ' and χ'' shift toward a higher temperature with increasing frequency f or, equivalently, decreasing the observation time $t=1/2\pi f$. The relaxation time for the thermally activated overbarrier relaxation of an isolated nanoparticle is given by $\tau \approx \tau_0 \exp(E_B/k_B T)$, where the energy barrier E_B is the uniaxial anisotropy energy barrier KV . K is the magnetocrystalline anisotropy, and V is the volume of a particle.

For an ensemble of noninteracting nanoparticles, χ'' curves can be used to determine the distribution of E_B by

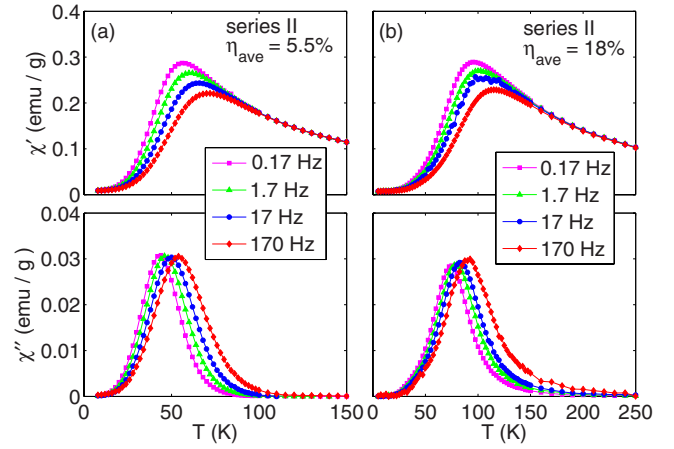


FIG. 2. (Color online) Temperature dependence of the in- and out-of-phase components of the ac susceptibility (χ' and χ'') of a film with (a) $\eta_{ave}=5.5\%$ and (b) $\eta_{ave}=18\%$ in series II.

plotting χ'' vs $E_b/k_B = -T \ln(2\pi f \tau_0)$.²⁶ These curves are independent of the measurement frequency if τ_0 is chosen correctly. For a sample with $\eta_{ave}=5.5\%$ in series II, $\tau_0=1 \times 10^{-14}$ s gives the best collapse of all χ'' curves measured at different frequencies. The resulting energy barrier distribution is shown in Fig. 3. The height of the χ'' peak for $\eta_{ave}=5.5\%$ is independent of f as expected for a noninteracting nanoparticle system. Hence, the dipolar interaction is relatively weak in this system and neglecting the dipolar interaction may be a crude approximation.

The energy barrier distribution is roughly consistent with an anisotropy-energy distribution only determined by the volume distribution. The estimated value of the anisotropy constant K coincides with that of the magnetocrystalline anisotropy of bulk fcc-Ni at low temperature, $K=8 \times 10^4$ J/m³.²⁷ This is consistent with the crystalline fcc-Ni

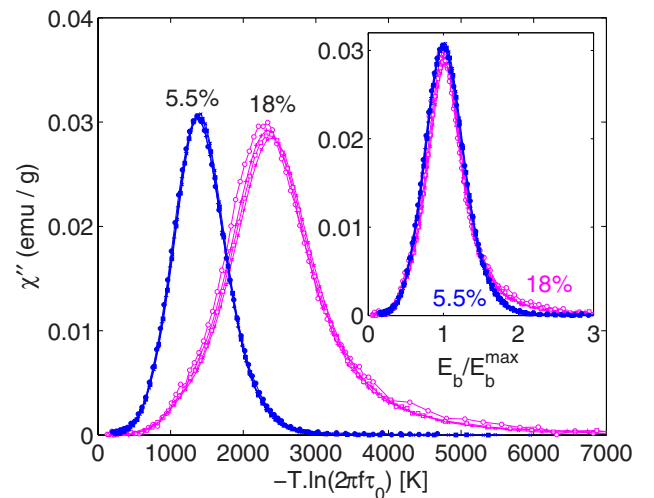


FIG. 3. (Color online) χ'' vs $E_b = -T \ln(2\pi f \tau_0)$ for the two samples with $\eta_{ave}=5.5\%$ (solid symbols) and $\eta_{ave}=18\%$ (open symbols) in series II. $\tau_0=1 \times 10^{-14}$ s was used both for the 5.5% and 18% samples. The inset illustrates the tail of large particles in the 18% sample by plotting χ'' vs E_b/E_b^{max} .

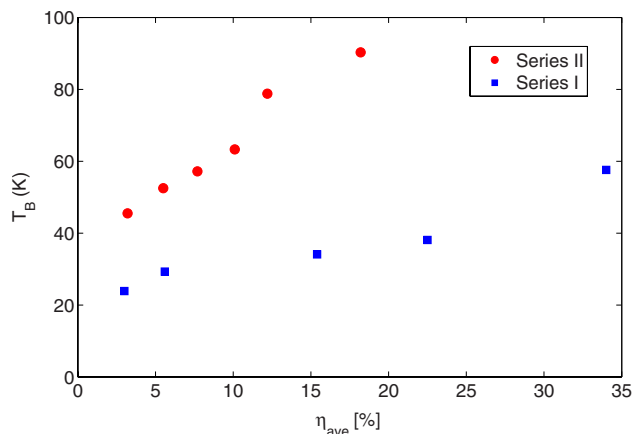


FIG. 4. (Color online) Blocking temperatures (T_B) as a function of particle volume fraction in the composite layer (η_{ave}). Squares and circles correspond to series I ($d_{ave} \sim 5$ nm) and II ($d_{ave} \sim 8$ nm), respectively.

observed by an electron diffraction pattern. For the sample with the lowest η_{ave} in series I, a similar analysis reveals the anisotropy constant $K \approx 13 \times 10^4$ J/m³, about a factor of 1.5 larger than for series II. This increase in anisotropy for the smaller particle size may be related to the increased surface-to-volume ratio for the smaller particles making the surface anisotropy important.

Temperature dependent measurements of the zero-field-cooled (ZFC) and field-cooled dc magnetizations were made for all samples. The probing magnetic field was 5 Oe, which is within the linear response regime. We identify the blocking temperature (T_B) with the maximum in the ZFC magnetization. Figure 4 shows T_B as a function of η_{ave} . Both series of samples exhibit the same trend: T_B increases with η_{ave} . The enhancement of T_B on decreasing the mean distance between particles has commonly been observed for various nanoparticle systems.^{6,7,12,13,15} The increase of T_B can be attributed to additional energy barriers created by the dipolar interaction.¹⁶ In the noninteracting limit ($\eta_{ave} \rightarrow 0$), considering that the time scale of the dc measurement is $\tau \sim 100$ s, the expression for the relaxation time yields $k_B T_B \approx KV / \ln(\tau / \tau_0) \approx KV / 35$. The values of the anisotropy constant obtained in this way are roughly consistent with those deduced from the ac susceptibility measurements.

In the range of strong dipolar interaction, a naive expectation is that the blocking temperature is proportional to the dipolar energy yielding $k_B T_B \propto \mu_0 M_s^2 V \eta_{ave}$. Comparing the two series, the slope of $T_B(\eta_{ave})$ is larger for series II than for series I as expected, and for both series, T_B is approximately linear with η_{ave} . However, a quantitative analysis according to this simple model cannot be made.

Figure 2(b) shows χ' and χ'' of a films with $\eta_{ave} = 18\%$ in series II. We note here that the peaks in the ac susceptibility appear at much higher temperatures compared to the 5.5% sample. In addition, the peak height of χ'' increases slightly with f , a commonly observed effect of the influence of dipolar interparticle interaction. An attempt to collapse the χ'' data using $\tau_0 = 1 \times 10^{-14}$ is shown in Fig. 3. The collapse is less good than for the 5.5% sample, especially at low tem-

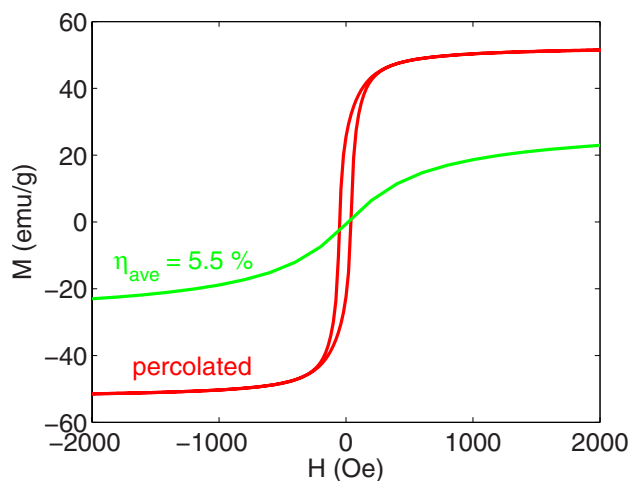


FIG. 5. (Color online) M - H hysteresis curves at 300 K for a sample with $\eta_{ave} = 5.5\%$ and the percolated sample in series II. The magnetic field is applied along the film. Demagnetization effects should therefore be small.

peratures, due to the increased importance of dipolar interparticle interaction. An even smaller $\tau_0 = 1 \times 10^{-16}$ s gives a bit better collapse of all χ'' curves. Such an unphysically²⁸ small value of τ_0 indicates the importance of dipolar interactions in the sample. We expect weak dipolar interactions to have slightly reduced the value of τ_0 also for the 5.5% sample.

In dense nanoparticle systems, strong dipolar interactions lead to spin-glass-like dynamics. In that case, new energy barriers are created dynamically by the frustrated dipolar interparticle interaction,¹⁶ and the onset of χ'' at the high temperature side becomes sharper than in a dilute sample.¹⁵ However, the χ'' curves for $\eta_{ave} = 18\%$ in Fig. 3 have a tail at the high temperature side, as can clearly be appreciated from the inset. This tail of large energy barriers indicates the existence of clusters of strongly exchange coupled particles behaving as one large entity. We note that in the present system, direct contact between particles is possible unlike for surfactant coated nanoparticles in a ferrofluid. It is thus plausible that in several parts of a sample, interparticle ferromagnetic exchange coupling dominates over the dipolar interaction in the range of large η . Thus, the tail of χ'' for $\eta_{ave} = 18\%$ can be regarded as a precursor of the percolation transition to a ferromagnet. According to a percolation theory, clusters of linear size $\xi \propto (\eta_c - \eta)^{-\nu}$ exist below the percolation threshold η_c . The critical exponent $\nu \approx 0.88$ in 3D systems, though we have not enough samples with η near η_c to check this divergent behavior. For a sample with η above η_c , we do expect direct exchange coupling between particles to be the dominating exchange mechanism.

Figure 5 shows magnetization versus magnetic field (M - H) hysteresis curves for samples in series II annealed for 30 min ($\eta_{ave} = 5.5\%$) and for 180 min (the continuous Ni film) at 300 °C. While the $\eta_{ave} = 5.5\%$ sample is superparamagnetic at this temperature, the percolated sample is ferromagnetic with a small coercivity of about 45 Oe. The saturation magnetization (M_s) of the continuous Ni film is close

to that for bulk Ni, 55 emu/g at 300 K, while it is lower, about 30 emu/g, for the dilute sample at the same temperature. A decrease in M_s for Ni nanoparticles has been reported²⁹ and can be attributed to surface effects. In accordance, M_s of the smaller sized nanoparticles in series I is even lower ($M_s \approx 26$ emu/g) compared to $M_s \approx 34$ emu/g for series II at low temperatures. It cannot be excluded that the particle surface is oxidized after the annealing process, which would explain the observed reduction of M_s . In addition, an enhanced magnetic anisotropy, as well as exchange-bias effects, is expected³⁰ in the case of a layer of antiferromagnet NiO on the surface of ferromagnetic Ni particles. An enhanced magnetic anisotropy is observed for the 5.6% sample of series I, while for samples both from series I and II, weak exchange-bias effects exist, consistent with NiO being formed on the particle surface. However, if the crystallinity of the surface layer is different from the fcc-Ni core, a reduced magnetic moment is also expected.³¹

IV. CONCLUSIONS

In conclusion, we have prepared PI films incorporating Ni nanoparticles. TEM studies demonstrated that the particle diameter d_{ave} and their volume fraction η_{ave} can be controlled independently. dc- and ac-magnetization measurements clearly show that the magnetic properties of these Ni nanoparticle systems can be controlled by tuning d_{ave} and η_{ave} . The samples with a low volume fractions of particles behave as ensembles of superparamagnets, as expected for noninter-

acting nanoparticle systems. With increasing η_{ave} , i.e., decreasing the mean interparticle distances, the dipolar interaction increases resulting in an enhanced T_B . For dense nanoparticle samples exhibiting spin-glass-like dynamics, the onset of χ'' is sharper than for noninteracting nanoparticle systems.¹⁵ However, the χ'' curves observed for $\eta_{ave}=18\%$ in the present study have a tail at the high temperature side. If the particle concentrations exceed the threshold for geometrical percolation, the magnetic response is ferromagnetic due to ferromagnetic exchange interactions between particle in direct contact. A tail at the high temperature side of the χ'' curves for the $\eta_{ave}=18\%$ sample can be interpreted as a precursor of such a critical percolation transition. The behavior of the investigated Ni nanoparticle systems is hence different from that of surfactant coated nanoparticle for which the minimum interparticle distance is limited by the surfactant. The magnetic properties of ferrofluids often change with time due to chain formation and clustering of the particles in a *liquid* medium. Here, we have shown that we can control the magnetic properties of this materials with single-domain particles dispersed three dimensionally in a *solid* matrix from superparamagnetic to ferromagnetic simply by changing the annealing time.

ACKNOWLEDGMENTS

The authors acknowledge M. Hagiwara, C. Mitsumata, H. Shinkai, Y. Tomita, and S. Ushioda for valuable discussions. S.T. was supported by PRESTO, JST.

*tomita@ms.naist.jp

[†]Present address: Department of Physics, Uppsala University, Box 530, SE-751 21 Uppsala, Sweden; petra.jonsson@fysik.uu.se

¹S. Chikazumi, *Physics of Ferromagnetism*, 2nd ed. (Oxford University Press, Oxford, 1997).

²S. Sun, C. B. Murray, D. Weller, L. Folks, and A. Moser, *Science* **287**, 1989 (2000).

³R. P. Cowburn and M. E. Welland, *Science* **287**, 1466 (2000).

⁴R. P. Cowburn, *Phys. Rev. B* **65**, 092409 (2002).

⁵S. Mørup and E. Tronc, *Phys. Rev. Lett.* **72**, 3278 (1994).

⁶J. L. Dormann, D. Fiorani, and E. Tronc, *Adv. Chem. Phys.* **98**, 283 (1997).

⁷F. Luis, F. Petroff, J. M. Torres, L. M. García, J. Bartolomé, J. Carrey, and A. Vaurès, *Phys. Rev. Lett.* **88**, 217205 (2002).

⁸J. L. García-Palacios, *Adv. Chem. Phys.* **112**, 1 (2000).

⁹S. T. Chui and L. Hu, *Phys. Rev. B* **65**, 144407 (2002).

¹⁰M. F. Hansen and S. Mørup, *Phys. Rev. Lett.* **90**, 059705 (2003); F. Luis, F. Petroff, J. M. Torres, L. M. Garcia, J. Bartolomé, J. Carrey, and A. Vaures, *ibid.* **90**, 059706 (2003).

¹¹W. Kleemann, O. Petravic, C. Binek, G. N. Kakazei, Y. G. Pogorelov, J. B. Sousa, S. Cardoso, and P. P. Freitas, *Phys. Rev. B* **63**, 134423 (2001).

¹²T. Jonsson, J. Mattsson, C. Djurberg, F. A. Khan, P. Nordblad, and P. Svedlindh, *Phys. Rev. Lett.* **75**, 4138 (1995).

¹³C. Djurberg, P. Svedlindh, P. Nordblad, M. F. Hansen, F. Bødker, and S. Mørup, *Phys. Rev. Lett.* **79**, 5154 (1997).

¹⁴S. Sahoo, O. Petravic, C. Binek, W. Kleemann, J. B. Sousa, S. Cardoso, and P. P. Freitas, *Phys. Rev. B* **65**, 134406 (2002).

¹⁵M. F. Hansen, P. Jönsson, P. Nordblad, and P. Svedlindh, *J. Phys.: Condens. Matter* **14**, 4901 (2002); P. E. Jönsson, *Adv. Chem. Phys.* **128**, 191 (2004).

¹⁶M. Sasaki, P. E. Jönsson, H. Takayama, and H. Mamiya, *Phys. Rev. B* **71**, 104405 (2005).

¹⁷O. Kitakami, H. Sato, Y. Shimada, F. Sato, and M. Tanaka, *Phys. Rev. B* **56**, 13849 (1997).

¹⁸J. P. Pierce, M. A. Torija, Z. Gai, J. Shi, T. C. Schulthess, G. A. Farnan, J. F. Wendelken, E. W. Plummer, and J. Shen, *Phys. Rev. Lett.* **92**, 237201 (2004).

¹⁹S. Tomita, M. Hagiwara, T. Kashiwagi, C. Tsuruta, Y. Matsui, M. Fujii, and S. Hayashi, *J. Appl. Phys.* **95**, 8194 (2004).

²⁰K. Akamatsu, H. Shinkai, S. Ikeda, S. Adachi, H. Nawafune, and S. Tomita, *J. Am. Chem. Soc.* **127**, 7980 (2005).

²¹S. Tomita, K. Akamatsu, H. Shinkai, S. Ikeda, H. Nawafune, C. Mitsumata, T. Kashiwagi, and M. Hagiwara, *Phys. Rev. B* **71**, 180414(R) (2005).

²²S. Tomita, K. Akamatsu, H. Shinkai, S. Ikeda, H. Nawafune, C. Mitsumata, T. Kashiwagi, and M. Hagiwara, in *Fabrication and New Applications of Nanomagnetic Structures*, edited by J.-P. Wang, P. J. Ryan, K. Nielsch, and Z. Cheng, MRS Symposia Proceedings No. 853E (Materials Research Society, Pittsburgh, 2005), p. I5.10.1.

²³M. Kiene, T. Strunskus, R. Peter, and F. Faupel, *Adv. Mater.*

- (Weinheim, Ger.) **10**, 1357 (1998).
- ²⁴S. Ikeda, K. Akamatsu, H. Nawafune, T. Nishino, and S. Deki, *J. Phys. Chem. B* **108**, 15599 (2004).
- ²⁵*Introduction to Percolation Theory*, edited by D. Stauffer and A. Aharony (Taylor & Francis, London, 1994).
- ²⁶T. Jonsson, J. Mattsson, P. Nordblad, and P. Svedlindh, *J. Magn. Mater.* **168**, 269 (1997).
- ²⁷H. J. Williams and R. M. Bozorth, *Phys. Rev.* **56**, 837 (1939).
- ²⁸The atomic spin-flip time is $\sim 1 \times 10^{-13}$ s, and τ_0 for a single nanoparticle is typically $\sim 1 \times 10^{-10} - \sim 1 \times 10^{-12}$ s.
- ²⁹Y. Wang, Q. Zhu, and H. Zhang, *J. Mater. Chem.* **16**, 1212 (2006).
- ³⁰V. Skumryev, S. Stoyanov, Y. Zhang, G. Hadjipanayis, D. Givord, and J. Nogués, *Nature (London)* **432**, 850 (2003).
- ³¹P. Pouloupoulos, V. Kapaklis, C. Politis, P. Schweiss, and D. Fuchs, *J. Nanosci. Nanotechnol.* **6**, 3867 (2006).